ChemComm

COMMUNICATION

View Article Online
View Journal | View Issue

Cite this: *Chem. Commun.*, 2024, **60**, 3409

Received 23rd January 2024,
Accepted 28th February 2024

DOI: 10.1039/d4cc00332b

rsc.li/chemcomm

Controllable synthesis of star-shaped $FeCoMnO_x$ nanocrystals and their self-assembly into superlattices with low-packing densities†

Zhe Xia,[a] Yutong Gao,[b] Qingfu Cai,[a] Yajun Wang,*[c] Dong Yang,*[a] Tongtao Li*[b] and Angang Dong*[b]

We present a novel method for synthesizing monodisperse, star-shaped $FeCoMnO_x$ nanocrystals with tunable concavity. Through liquid–air interfacial assembly, these colloidal nanostars can form two-dimensional superlattices, which are characterized by low packing densities. Notably, the ability to adjust the degree of concavity of nanostars allows for the tuning of the packing symmetry of the assembled superlattices.

The self-assembly of colloidal nanocrystals (NCs) into ordered arrays or superlattices is a burgeoning area of research due to its potential for creating materials with unique collective properties.[1–3] Recent advancements in colloidal synthesis techniques have facilitated the production of monodisperse NCs with varying compositions, sizes, and shapes.[4–6] As a result, there has been a surge of interest in the bottom-up assembly of two-dimensional (2D) and three-dimensional (3D) superlattices with intricate structures.[7–9] Traditional superlattices formed from spherical NCs exhibit close-packed structures with the densest packing configurations.[10,11] Recently, there has been a growing interest in designing porous, non-close-packed superlattice materials due to their ability to enhance mass transport and guest species accessibility, thereby expanding their potential applications in catalysis, energy storage, and sensing.[12,13] Consequently, considerable attention has been directed towards the design and assembly of superlattice materials with low packing densities. Several notable efforts have been made in this field. For example, Yang and coworkers confined the self-assembly of NCs within nanotubes to create NC superstructures with open features.[14] Mirkin's group has developed open-channel superlattice frameworks based on the self-assembly of hollow NC frames.[15] Additionally, the self-assembly of trigonal bipyramidal NCs has led to the formation of open-framework cage structures.[16] Despite these significant advances, previous research has predominantly focused on the assembly of convex NCs, with limited exploration in utilizing concave NC building blocks for constructing superlattice materials.[17–19]

There have been some encouraging advances in the self-assembly of micron-sized colloids with concave features. For instance, Liu and colleagues demonstrated the formation of a unique 2D open superstructure using biconcave polystyrene discs.[20] Weck *et al.* achieved flexible bonding of "lock" and "key" particles by preparing colloids with well-defined multicavities.[21] These studies have provided insights into the self-assembly dynamics of colloidal NCs with concave features.[22] To explore the self-assembly behaviors of colloidal NCs with concave features, it is necessary to synthesize high-quality concave NCs with tailored shapes. While there have been successful efforts in creating metal oxide NCs with various morphologies,[23,24] the controlled synthesis of concave metal oxide NCs with tunable degrees of concavity remains challenging.

In this work, we have successfully synthesized star-shaped $FeCoMnO_x$ NCs with excellent colloidal stability and monodispersity. These star-shaped $FeCoMnO_x$ NCs prove to be versatile concave building blocks for the self-assembly of 2D superlattices with two types of packing symmetries, both of which are characterized by low-packing densities that are enabled by the concave nature of $FeCoMnO_x$ NCs. By employing a drying-mediated assembly approach at the liquid–air interface, we achieve the formation of long-range ordered superlattice membranes. These 2D superlattice membranes can be easily transferred onto arbitrary substrates for further structural characterization. Importantly, through the optimization of synthetic conditions, we can modulate the degree of concavity in $FeCoMnO_x$ NCs, which proves to be a key factor in tuning the packing symmetry of the resulting superlattices. This work not

[a] *State Key Laboratory of Molecular Engineering of Polymers and Department of Macromolecular Science, Fudan University, Shanghai 200433, China*
[b] *Shanghai Key Laboratory of Molecular Catalysis and Innovative Materials and Department of Chemistry, Fudan University, Shanghai 200433, China*
[c] *College of Chemistry and Materials Engineering, Wenzhou University, Wenzhou 325027, China*

† Electronic supplementary information (ESI) available. See DOI: https://doi.org/10.1039/d4cc00332b

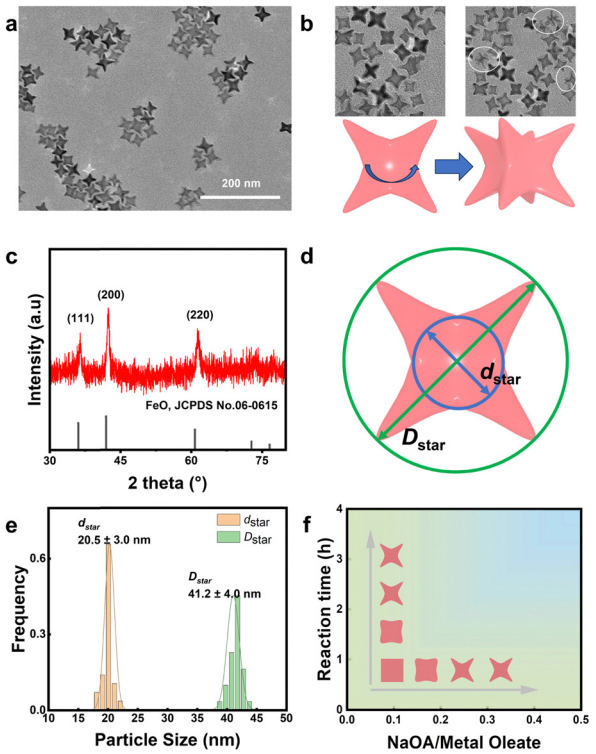

Fig. 1 (a) TEM and (b) tilted TEM images, and (c) XRD pattern of star-shaped $FeCoMnO_x$ NCs. (d) Schematic showing the shape parameter of star-shaped NCs. (e) D and d distribution of star-shaped $FeCoMnO_x$ NCs with D/d = 2.0. (f) Diagrammatic representation illustrating the shape evolution of $FeCoMnO_x$ NCs as a function of NaOA to metal oleate ratio and reaction time.

only demonstrates the colloidal synthesis of monodisperse star-shaped NCs with controllable concavity but also introduces a novel approach for constructing superlattice materials with low-packing densities.

In this study, colloidal $FeCoMnO_x$ nanostars, capped with oleic acid ligands, are synthesized by decomposing a mixed-metal oleate precursor and sodium oleate (NaOA) at 315 °C (see details in ESI†). Fig. 1a presents the transmission electron microscopy (TEM) image of typical star-shaped $FeCoMnO_x$ NCs, showing their remarkable uniformity in both size and shape. The tilted TEM images in Fig. 1b reveal that each star consists of a central core and eight pyramidal arms, presumably extending from the eight corners of a nanocube. As a result, each star is characterized by six equivalent concave surfaces with twelve concave edges. X-ray diffraction (XRD) verifies the crystalline nature of the nanostars (Fig. 1c), which exhibit a wüstite crystal structure.[23] To quantitatively describe the shape of $FeCoMnO_x$ stars, we introduce two geometric parameters, d and D. Here, D represents the diameter of the larger circle that is internally tangent to the arm tips, while d corresponds to the diameter of the smaller circle externally tangent to the concave surface (Fig. 1d). The ratio between D and d (D/d) effectively quantifies the degree of concavity of $FeCoMnO_x$ stars. It should be noted that cubic NCs, without concave surfaces, have a D/d ratio of approximately 1.4. Statistical analysis shows that the average d of typical $FeCoMnO_x$ stars is 20.5 ± 3.0 nm with an average D of 41.2 ± 4.0 nm (Fig. 1e), thus giving rise to a D/d ratio of 2.0.

The experimental parameters that affect the growth of $FeCoMnO_x$ stars have been systematically investigated. It was found that NaOA is crucial for achieving monodisperse nanostars, as $FeCoMnO_x$ NCs undergo a morphological evolution from rounded cubes to star shapes as the NaOA to metal oleate precursor ratio (NaOA/metal oleate) varies from 0.1 to 0.5 (Fig. S1a–c, ESI†). The duration of the reaction also significantly impacts the growth of star-shaped NCs. Initial stages show the presence of spherical and cubic NCs, which gradually evolve into stars (Fig. S1d–f, ESI†). These observations are summarized in a diagram in which the two trends are highlighted. As illustrated in Fig. 1f, improving the NaOA to metal oleate ratio induces a morphological evolution from cubes to stars, provided that the reaction time is held constant. On the other hand, maintaining a constant NaOA/metal oleate ratio while prolonging the reaction time promotes the preferential enlargement of stars. Additionally, our experiments reveal star-shaped NCs are predominantly formed at lower temperatures (310–315 °C), while elevated temperatures (>320 °C) tend to yield spherical and cubic NCs (Fig. S1g–i, ESI†). This observation suggests that the growth of star-shaped NCs is governed mainly by kinetic control.[24]

Besides the concave geometry, another notable feature of these $FeCoMnO_x$ stars is their remarkable colloidal stability when dispersed in nonpolar solvents such as hexane. The colloidal solution of $FeCoMnO_x$ stars remains stable without noticeable aggregation for several weeks, despite their relatively large size. This colloidal stability is largely attributed to the presence of oleic acid ligands attached to the surface of $FeCoMnO_x$ stars. The combination of high colloidal stability and size uniformity of $FeCoMnO_x$ stars is crucial for subsequent self-assembly.

We employ a liquid–air interfacial assembly technique to investigate the self-assembly behaviors of $FeCoMnO_x$ NCs with varying D/d ratios.[25] The self-assembly experiments are conducted by drop-casting a hexane solution containing $FeCoMnO_x$ NCs onto the surface of diethylene glycol (DEG). The subsequent evaporation of the solvent initiates the formation of 2D superlattice monolayers, the packing configuration of which is highly dependent on the D/d ratio. TEM reveals that cubic $FeCoMnO_x$ NCs, with a D/d ratio of 1.4, self-assemble into squarely-packed superlattices ($p4m$ wallpaper symmetry) with high packing densities (Fig. 2a and b). On the other hand, $FeCoMnO_x$ stars are found to exhibit different assembly behaviors, depending on their degree of concavity. Self-assembly of $FeCoMnO_x$ stars with less concavity (D/d = 1.6) tend to form disordered structures with short-range square packing arrangement (Fig. 2c and d), while exploiting $FeCoMnO_x$ stars with a D/d ratio of 1.8 for self-assembly leads to the formation of long-range ordered superlattices composed of close-packed stars (Fig. 2e). The domain size of the obtained star superlattices can reach several micrometers (Fig. S2, ESI†). These comparative studies suggest that a higher degree of concavity in stars is

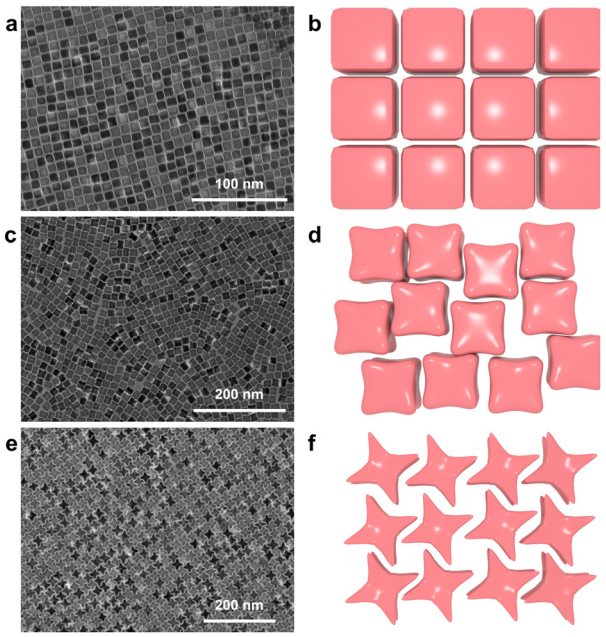

Fig. 2 TEM images and corresponding structural models of the assemblies formed from $FeCoMnO_x$ NCs with different D/d ratios: (a) and (b) D/d = 1.4, (c) and (d) D/d = 1.6, (e) and (f) D/d = 1.8.

essential for promoting their ordered assembly into superlattices. For $FeCoMnO_x$ stars with a lower degree of concavity, they lack the ability to effectively interlock, which can frustrate their long-range ordered assembly.

The observed closed-packed configuration in the star superlattices is largely attributed to the local shape complementarity between convex arms and concave surfaces of adjacent $FeCoMnO_x$ stars, as depicted in the structural model (Fig. 2f). Closer inspection by high-resolution TEM (HRTEM, Fig. 3a) indicates that these stars, oriented on four of their arms, are arranged to form a square lattice with a *p*4 wallpaper symmetry.[26] The presence of the four-fold symmetry is further confirmed by small-angle electron diffraction (SAED, Fig. 3b). The long-range

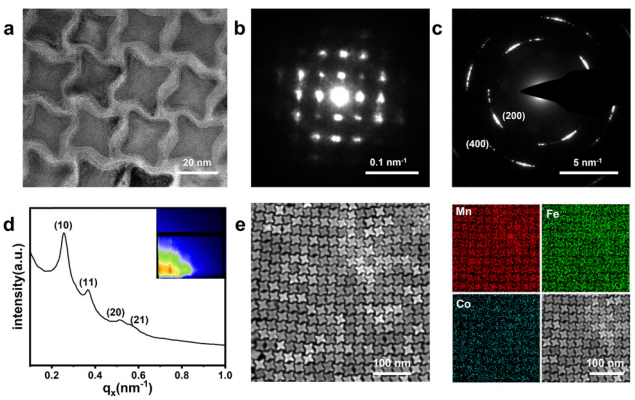

Fig. 3 (a) HRTEM image, (b) SAED pattern, (c) WAED pattern, (d) GISAXS pattern and 2D diffusion rings (inset), and (e) HAADF-STEM image and elemental mapping of *p*4-type superlattices self-assembled from $FeCoMnO_x$ stars with D/d = 1.8.

structural order of the *p*4-type superlattices is corroborated by the grazing-incidence small-angle X-ray scattering (GISAXS) pattern, which shows scattering peaks characteristic of a square lattice (Fig. 3d).[27,28] High-angle annular dark-field scanning TEM and corresponding elemental mapping (HAADF-STEM, Fig. 3e) further illustrate the square arrangement of $FeCoMnO_x$ stars in the *p*4-type superlattices. The 2D packing density (ρ) of these *p*4-type superlattices can be calculated by treating each star as a cross, which is approximately 0.61 considering the presence of a layer of oleic acid ligands on the surface of stars (Note S1, ESI†). Notably, this packing density is significantly lower than that of 2D superlattices formed from spherical NCs, which have a packing density of 0.906.[29] Presumably, the low packing density of the *p*4-type superlattices is due to the interstitial voids between adjacent stars. The wide-angle electron diffraction (WAED) pattern of these star superlattices displays four broad arcs corresponding to (200) reflections of $FeCoMnO_x$ NCs (Fig. 3c). This indicates that the stars within the superlattices are not perfectly aligned, which could be a consequence of their relatively low packing density.

To explore the origin of the structural transition from *p*4*m*-type to *p*4-type with an increase of the degree of concavity, we calculate the space-filling curve of the corresponding structure. This can be achieved by plotting the packing density of the superlattice as a function of the parameter h/D, where h represents the depth of the concave surface (see Fig. S4 for calculation details, ESI†). As indicated by Fig. S4 (ESI†), when h/D is less than 0.1, the packing density of the *p*4*m*-type superlattice is higher than that of the *p*4-type superlattice. This suggests that the *p*4*m*-type superlattice is the preferential structure when using NCs with less concavity. However, as h/D increases further, the *p*4-type superlattices become favoured due to their higher packing density. These findings are in good agreement with the structural transition observed in our experiments, highlighting the significant role of entropy in the self-assembly process.

Interestingly, self-assembly of $FeCoMnO_x$ stars with a further increased degree of concavity leads to a transition of *p*4-type superlattices to *p*6*m*-type superlattices. Fig. 4a shows the TEM image of such *p*6*m*-type superlattices formed from $FeCoMnO_x$ stars with a D/d ratio of 2.0, the typical domain size of which is several micrometers. The six-fold symmetry of *p*6*m*-type superlattices is verified by HRTEM (Fig. 4b) and SAED (Fig. 4c). The orientation of the stars within the hexagonal superlattices is such that one pyramidal arm rests on the substrate, while the opposite arm projects upward, as confirmed by the bright spots observed in scanning electron microscopy (SEM, Fig. 4d) and HAADF-STEM (Fig. 4e). Furthermore, the HAADF-STEM image in Fig. 4e clearly demonstrates the porous nature of *p*6*m*-type superlattices as depicted in the structural model (Fig. 4f). For each star (green star in Fig. 4f), its three arms at the same height are complementary to the concave surfaces of three neighboring stars (blue stars in Fig. 4f), while its three concave surfaces complement the arms of three adjacent stars (red stars in Fig. 4f), effectively stabilizing the formed superlattice. It is interesting to note that in some cases, bilayer *p*6*m*-type superlattices are observed, where the second layer of stars fills the interstices of the first layer (Fig. S3, ESI†). The

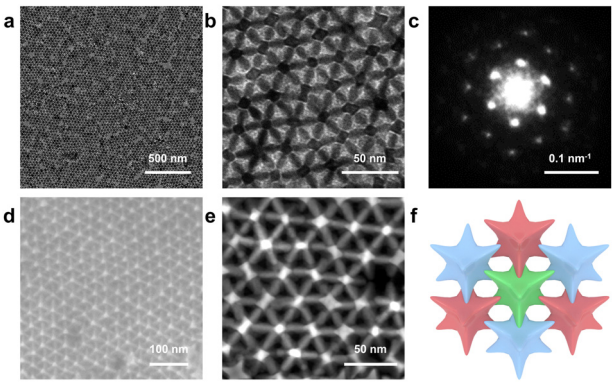

Fig. 4 (a) TEM image, (b) HRTEM image, (c) SAED pattern, (d) SEM image, (e) HAADF-STEM image, and (f) structural model of *p6m*-type superlattices.

transition from *p4*-type to *p6m*-type superlattices is attributable to the variation in the *D*/*d* ratios of $FeCoMnO_x$ stars that construct them. We hypothesize that at *D*/*d* = 1.8, the lesser concavity of stars facilitates their arrangement with the arms of adjacent stars oriented in a parallel manner (Fig. 2f), leading to the formation of a square lattice. As the *D*/*d* ratio increases, the packing density of the square superlattice decreases, which, in turn, promotes the organization of stars into a hexagonal symmetry. Moreover, at *D*/*d* = 2.0, the elongated arms of stars can effectively facilitate their interaction with the concave surfaces, thereby stabilizing the *p6m*-type superlattice structure.

In conclusion, we have developed the colloidal synthesis of monodisperse, star-shaped $FeCoMnO_x$ NCs featuring well-defined concave geometry and excellent colloidal stability. By adjusting the reaction conditions, we are able to finely control the degree of concavity in these colloidal nanostars, without compromising their size monodispersity and colloidal stability. This allows us to systematically investigate the concavity-dependent assembly behaviors of colloidal NCs. We observe the emergence of two types of monolayer superlattices, both characterized by low packing densities, upon the liquid–air interfacial assembly of $FeCoMnO_x$ stars with different degrees of concavity. This work offers a new route for designing superlattice materials with low packing densities, which could find wide applications in catalysis, energy storage, and sensing.

This work was supported by National Key Research and Development Program of China (2022YFA1503501), NSFC (52333013, 22025501, 22088101, 22175132, 52202088, 52373204), Shanghai Municipal Science and Technology Project (23JC1400100, 21520713800), and the Fundamental Research Funds for the Central Universities (20720220010).

Conflicts of interest

There are no conflicts to declare.

Notes and references

1 M. A. Boles, M. Engel and D. V. Talapin, *Chem. Rev.*, 2016, **116**, 11220–11289.
2 M. S. Lee, D. W. Yee, M. Ye and R. J. Macfarlane, *J. Am. Chem. Soc.*, 2022, **144**, 3330–3346.
3 Z. Li, Q. Fan and Y. Yin, *Chem. Rev.*, 2022, **122**, 4976–5067.
4 Q. N. Nguyen, C. Wang, Y. Shang, A. Janssen and Y. Xia, *Chem. Rev.*, 2023, **123**, 3693–3760.
5 A. Walther and A. H. Muller, *Chem. Rev.*, 2013, **113**, 5194–5261.
6 Y. Wang, J. Chen, R. Li, A. Gotz, D. Drobek, T. Przybilla, S. Hubner, P. Pelz, L. Yang, B. Apeleo Zubiri, E. Spiecker, M. Engel and X. Ye, *J. Am. Chem. Soc.*, 2023, **145**, 17902–17911.
7 S. Yang, R. A. LaCour, Y.-Y. Cai, J. Xu, D. J. Rosen, Y. Zhang, C. R. Kagan, S. C. Glotzer and C. B. Murray, *J. Am. Chem. Soc.*, 2023, **145**, 6280–6288.
8 Y. Yang, B. Wang, X. Shen, L. Yao, L. Wang, X. Chen, S. Xie, T. Li, J. Hu, D. Yang and A. Dong, *J. Am. Chem. Soc.*, 2018, **140**, 15038–15047.
9 Y. Nagaoka, R. Tan, R. Li, H. Zhu, D. Eggert, Y. A. Wu, Y. Liu, Z. Wang and O. Chen, *Nature*, 2018, **561**, 378–382.
10 K. Deng, Z. Luo, L. Tan and Z. Quan, *Chem. Soc. Rev.*, 2020, **49**, 6002–6038.
11 I. Cherniukh, G. Rainò, T. V. Sekh, C. Zhu, Y. Shynkarenko, R. A. John, E. Kobiyama, R. F. Mahrt, T. Stöferle, R. Erni, M. V. Kovalenko and M. I. Bodnarchuk, *ACS Nano*, 2021, **15**, 16488–16500.
12 T. Li, B. Xue, B. Wang, G. Guo, D. Han, Y. Yan and A. Dong, *J. Am. Chem. Soc.*, 2017, **139**, 12133–12136.
13 A. G. Slater and A. I. Cooper, *Science*, 2015, **348**, aaa8075.
14 F. Zhang, R. Liu, Y. Wei, J. Wei and Z. Yang, *J. Am. Chem. Soc.*, 2021, **143**, 11662–11669.
15 Y. Li, W. Zhou, I. Tanriover, W. Hadibrata, B. E. Partridge, H. Lin, X. Hu, B. Lee, J. Liu, V. P. Dravid, K. Aydin and C. A. Mirkin, *Nature*, 2022, **611**, 695–701.
16 H. Lin, S. Lee, L. Sun, M. Spellings, M. Engel, S. C. Glotzer and C. A. Mirkin, *Science*, 2017, **355**, 931–935.
17 Y. Liu, K. Deng, J. Yang, X. Wu, X. Fan, M. Tang and Z. Quan, *Chem. Sci.*, 2020, **11**, 4065–4073.
18 S. Wan, X. Xi, H. Zhang, J. Ning, Z. Zheng, Z. Zhang, Y. Long, Y. Deng, P. Fan, D. Yang, T. Li and A. Dong, *ACS Nano*, 2022, **16**, 21315–21323.
19 Q. Wang, Z. Wang, Z. Li, J. Xiao, H. Shan, Z. Fang, and L. Qi, *Sci. Adv.*, 2017, **8**, eabo2626.
20 S. Li, J. He, S. Qiao, X. Zhang and B. Liu, *Small*, 2023, **19**, e2300642.
21 Y. Wang, Y. Wang, X. Zheng, G. R. Yi, S. Sacanna, D. J. Pine and M. Weck, *J. Am. Chem. Soc.*, 2014, **136**, 6866–6869.
22 C. Liu, Z. Ou, F. Guo, B. Luo, W. Chen, L. Qi and Q. Chen, *J. Am. Chem. Soc.*, 2020, **142**, 11669–11673.
23 A. Feld, A. Weimer, A. Kornowski, N. Winckelmans, J. P. Merkl, H. Kloust, R. Zierold, C. Schmidtke, T. Schotten, M. Riedner, S. Bals and H. Weller, *ACS Nano*, 2019, **13**, 152–162.
24 Z. Zhao, Z. Zhou, J. Bao, Z. Wang, J. Hu, X. Chi, K. Ni, R. Wang, X. Chen, Z. Chen and J. Gao, *Nat. Commun.*, 2013, **4**, 2266.
25 A. Dong, J. Chen, P. M. Vora, J. M. Kikkawa and C. B. Murray, *Nature*, 2010, **466**, 474–477.
26 L. Liu, G. P. T. Choi and L. Mahadevan, *Proc. R. Soc. London Ser. A*, 2021, **477**, 20210161.
27 C. Y. Zheng, Y. Yao, J. Deng, S. Seifert, A. M. Wong, B. Lee and C. A. Mirkin, *ACS Nano*, 2022, **16**, 4813–4822.
28 S. C. Boehme, M. I. Bodnarchuk, M. Burian, F. Bertolotti, I. Cherniukh, C. Bernasconi, C. Zhu, R. Erni, H. Amenitsch, D. Naumenko, H. Andrusiv, N. Semkiv, R. A. John, A. Baldwin, K. Galkowski, N. Masciocchi, S. D. Stranks, G. Raino, A. Guagliardi and M. V. Kovalenko, *ACS Nano*, 2023, **17**, 2089–2100.
29 A. Dong, X. Ye, J. Chen and C. B. Murray, *Nano Lett.*, 2011, **11**, 1804–1809.